

Spectroscopic Studies of the Mononuclear Non-Heme Fe^{II} Enzyme FIH: Second-Sphere Contributions to Reactivity

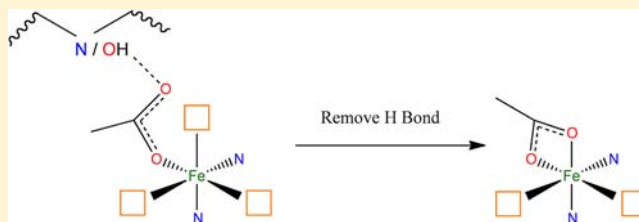
Kenneth M. Light,[†] John A. Hangasky,[‡] Michael J. Knapp,[‡] and Edward I. Solomon^{*,†}

[†]Department of Chemistry, Stanford University, Stanford, California 94305, United States

[‡]Department of Chemistry, University of Massachusetts, Amherst, Massachusetts 01003, United States

S Supporting Information

ABSTRACT: Factor inhibiting hypoxia-inducible factor (FIH) is an α -ketoglutarate (α KG)-dependent enzyme which catalyzes hydroxylation of residue Asn803 in the C-terminal transactivation domain (CAD) of hypoxia-inducible factor 1 α (HIF-1 α) and plays an important role in cellular oxygen sensing and hypoxic response. Circular dichroism (CD), magnetic circular dichroism (MCD), and variable-temperature, variable-field (VTVH) MCD spectroscopies are used to determine the geometric and electronic structures of FIH in its (Fe^{II}), (Fe^{II}/ α KG), and (Fe^{II}/ α KG/CAD) forms. (Fe^{II})FIH and (Fe^{II}/ α KG)FIH are found to be six-coordinate (6C), whereas (Fe^{II}/ α KG/CAD)FIH is found to be a 5C/6C mixture. Thus, FIH follows the general mechanistic strategy of non-heme Fe^{II} enzymes. Modeling shows that, when Arg238 of FIH is removed, the facial triad carboxylate binds to Fe^{II} in a bidentate mode with concomitant lengthening of the Fe^{II}/ α KG carbonyl bond, which would inhibit the O₂ reaction. Correlations over α -keto acid-dependent enzymes and with the extradiol dioxygenases show that members of these families (where both the electron source and O₂ bind to Fe^{II}) have a second-sphere residue H-bonding to the terminal oxygen of the carboxylate, which stays monodentate. Alternatively, structures of the pterin-dependent and Rieske dioxygenases, which do not have substrate binding to Fe^{II}, lack H-bonds to the carboxylate and thus allow its bidentate coordination which would direct O₂ reactivity. Finally, vis-UV MCD spectra show an unusually high-energy Fe^{II} \rightarrow α KG π^* metal-to-ligand charge transfer transition in (Fe^{II}/ α KG)FIH which is red-shifted upon CAD binding. This red shift indicates formation of H-bonds to the α KG that lower the energy of its carbonyl LUMO, activating it for nucleophilic attack by the Fe–O₂ intermediate formed along the reaction coordinate.



1. INTRODUCTION

Oxygen-activating mononuclear non-heme iron enzymes catalyze the reactions of a wide variety of organic substrates with O₂ with relevance to health, pharmaceuticals, and environmental remediation.^{1,2} These enzymes utilize an Fe^{II} center which directly binds O₂ to form iron–oxygen intermediates competent for reaction with substrate. As the one-electron reduction of O₂ to form an Fe^{III}–O₂[−] species is thermodynamically unfavorable,³ these enzymes also utilize a cofactor or redox-active substrate as a source of the additional electrons needed for O₂ activation. The majority of oxygen-activating mononuclear non-heme iron enzymes may be divided into four families on the basis of the source of additional electrons to generate the oxidizing intermediate.⁴ Rieske dioxygenases utilize one electron from a Rieske [2Fe–2S] cluster close to the mononuclear active site and connected through a hydrogen-bond (H-bond) network. Pterin-dependent hydroxylases require a tetrahydrobiopterin (BH₄) cofactor bound in the active site pocket, though not covalently bound to Fe^{II}. Extradiol dioxygenases coordinate catechol substrates to Fe^{II} in a bidentate fashion and catalyze their ring cleavage (the catecholate providing the extra electrons required for reactivity). α -Ketoglutarate-dependent (α KG-dependent) oxygenases use a coordinated α KG which binds bidentate to Fe^{II}.

All four of these families utilize a 2-His-1-carboxylate facial triad motif of amino acid-derived ligands for Fe complexation.^{5–7}

Factor inhibiting hypoxia-inducible factor, FIH, is an α KG-dependent asparaginyl hydroxylase involved in sensing hypoxia within the cells of humans and other animals.⁸ Its substrate is the C-terminal activation domain (CAD) of the hypoxia-inducible factor 1 α (HIF-1 α), one subunit of a heterodimeric transcription factor protein. HIF-1 α controls over 100 genes involved in increased O₂ delivery to the cell, including those associated with production of erythropoietin for increased red blood cell production and vascular endothelial growth factor, which is a major stimulant for angiogenesis.^{9–12} As long as sufficient O₂ is present, FIH will hydroxylate Asn803 of HIF-1 α . This hydroxylation prevents binding of the transcriptional coactivators p300 or CPB (Cyclic adenosine monophosphate response element-Binding-Protein) to HIF-1 α which is required for gene activation.^{13–15} Once O₂ concentrations within the cell drop to a sufficient level, Asn803 of HIF-1 α is no longer hydroxylated, and the hypoxic response commences. Although HIF-1 α is composed of over 800 residues and has not been made in sufficient quantity for biochemical studies, a CAD

Received: December 24, 2012

Published: June 6, 2013

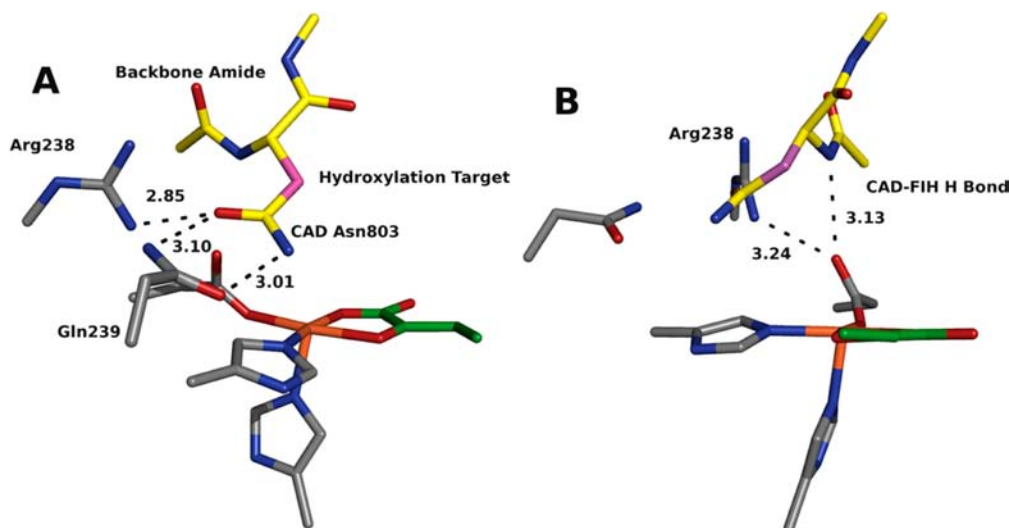


Figure 1. Views of the CAD-bound FIH Fe^{II} active site from crystal structure 1H2L showing (A) H-bonds between the CAD Asn803 amide and the FIH residues Arg238 and Gln239 and (B) H-Bonds between the FIH facial triad carboxylate and FIH Arg238 and the CAD Val802-Asn803 backbone amide. The C atoms of the FIH and CAD residues are colored gray and yellow, respectively, with the exception of the site of CAD hydroxylation, which is colored magenta. The C atoms of the bound α KG are colored green (the carboxylate tail has been removed). All distances are in Å.

fragment containing approximately 40 residues has been shown to be hydroxylated by FIH at the appropriate position in Asn803.^{16,17} The relatively small size of this substrate compared to the full protein may lead to the deletion of a number of substrate/enzyme interactions which, as of this time, have not been tested, and increasing the size of the CAD substrate does have an effect on k_{cat} and K_m .¹⁸ However, FIH can hydroxylate the CAD fragment *in vitro* on a reasonable time scale (20 min) at the correct position of Asn803 with >10:1 coupled:uncoupled turnover,¹⁵ indicating that this truncated substrate is a reasonable model for biochemical studies.

α -Ketoglutarate-dependent enzymes follow a general mechanistic strategy in which the Fe^{II} site is six-coordinate (6C) when the active site is devoid of substrate or α KG cofactor (in its “resting” form), the Fe^{II} being coordinated to the facial triad and three water ligands. α -Ketoglutarate displaces two of the water ligands to coordinate bidentate to the Fe^{II}. In this form the site remains 6C, which limits reaction of the Fe^{II} α KG site with O₂ before substrate is in position. Substrate binding leads to release of the remaining water ligand, thereby opening a coordination site for reaction with O₂.^{19,20} For example, in the case of halogenase SyrB2, the rate of reaction of the substrate-bound complex with O₂ is ~5000 times faster than that of the substrate-free form.²¹ Another example from a different non-heme Fe^{II} enzyme family is found in the pterin-dependent enzyme tyrosine hydroxylase, where the rate of O₂ binding to the 5C pterin/substrate-bound form is ~200 times faster than that of the 6C site in the absence of substrate.²² Reaction with O₂ before substrate and cofactor are in place can lead to uncoupled turnover as well as self-hydroxylation of the enzyme which has been observed in several α KG-dependent proteins when α KG is bound and substrate is absent.^{23–25} In the case of 1-aminocyclopropane-1-carboxylic acid oxidase (ACCO) binding of 1-aminocyclopropane-1-carboxylic acid in the absence of CO₂/HCO₃⁻ leads to a 5C site²⁶ which reacts with O₂ to form Fe^{III} and generates almost no ethylene product.²⁷ In the presence of CO₂/HCO₃⁻ the site will remain 6C until the cofactor ascorbate also binds.²⁶ These findings point to the

importance of forming a 5C Fe^{II} site only when all of the necessary components are in place for coupled reaction.

The active site of α KG/CAD-bound FIH ((Fe^{II}/ α KG/CAD)FIH) as determined by crystallography is shown in Figure 1¹⁶ where the key second-sphere interactions are H-bonds from the backbone amide of Asn803 of CAD and from the side chain of FIH Arg238. In this figure the majority of CAD C atoms are colored yellow. Asn803 of the CAD substrate is held in place above the Fe^{II} through H-bonds with FIH residues Arg238 and Gln239 as shown in Figure 1A. The β -carbon of CAD Asn803 (colored magenta) is the target for hydroxylation and is poised directly above the Fe^{II} atom. The CAD Val802-Asn803 backbone amide N–H group H-bonds with the facial triad carboxylate as shown in Figure 1B. In the absence of substrate, H-bonding between the facial triad carboxylate and the coordinated water in the α KG-bound form of α KG-dependent enzymes strengthens the Fe–OH₂ bond by giving the water partial hydroxide character.²⁸ When this H-bond cannot be formed, such as in TauD where the carboxylate of the facial triad is tilted down and in the halogenases CytC3 and SyrB2 which have halide ions in place of the facial triad carboxylate, an alternative enzyme residue H-bonds to coordinated water which helps keep it bound to the Fe^{II} active site.²⁸ In CAD-bound FIH, the substrate amide facial triad carboxylate H-bond may therefore serve a purpose in weakening the Fe–OH₂ bond by competing with the coordinated water for the facial triad carboxylate O not coordinated to Fe^{II} and thus help to induce water loss. The contributions of substrate H-bonding and steric clashes to loss of coordinated H₂O in NH Fe^{II} enzymes will be presented elsewhere.²⁹ It is also interesting to note that the facial triad carboxylate is tilted toward Arg238 both in the presence and absence of CAD substrate (Figure 1B). This carboxylate orientation implies an additional H-bond interaction, which also may serve to weaken the carboxylate–water H-bond mentioned above.

In contrast to the general mechanistic strategy described above, crystal structures for (Fe^{II}/ α KG)FIH in the absence of CAD do not give definitive evidence for the presence or

absence of a coordinated water ligand.^{16,30} EPR spectroscopic studies of (Co^{II}/αKG)FIH indicated that this form is a 5C/6C mixture.²⁵ Such behavior has not been observed for other members of the family, and a 5C (Fe^{II}/αKG)FIH site would lead to uncoupled turnover and potential deactivation of the enzyme. Our laboratory has developed a methodology utilizing near-infrared (NIR) circular dichroism (CD), magnetic circular dichroism (MCD), and variable-temperature, variable-field (VTVH) MCD spectroscopies to obtain detailed ligand field information about the geometric and electronic structures of Fe^{II} sites in proteins in solution.^{31,32} In the present study this methodology (outlined at the beginning of the Results section) has been utilized to evaluate the mechanistic strategy of FIH in comparison to that of other αKG-dependent enzymes. We have also used vis/UV MCD spectroscopy to obtain insight into the metal-to-ligand charge transfer (MLCT) transitions present for the αKG-bound forms of members of this enzyme family, most notably clavamate synthase 2 (CS2).^{28,33,34} Vis/UV MCD spectroscopy has been used here to analyze the electronic structures of the αKG- and αKG/CAD-bound forms of FIH which show large differences relative to the other αKG enzymes studied and coupled with density functional theory (DFT) calculations provide insight into how second-sphere interactions tune the reactivity of the Fe^{II}/αKG moiety toward reaction with O₂. These calculations also provide important new insight into how the second-sphere Arg238 interaction in Figure 1B tunes the reactivity of the Fe^{II} active site both specifically in FIH and generally over all four classes of oxygen-activating non-heme iron enzymes.

2. MATERIALS AND METHODS

Sample Preparation. Recombinant human FIH and HIF-1α CAD 39-mer were expressed and purified as described previously.²⁵ The CAD substrate corresponded to human HIF-1α residues 788–826, with a C800A point mutation to prevent spurious oxidation reactions: DESGLPQLTSYDAEVNAPIQGSRNLLQGEELLRALDQVN. The CAD peptide was purchased as a desalted peptide from EZBiolab (Carmel, IN, U.S.A.) with free N- and C-termini. RP-HPLC utilizing a gradient from 30% acetonitrile/0.1% trifluoroacetic acid (TFA) to 95% acetonitrile/0.1% TFA was used to obtain CAD of >95% purity. Apo-FIH was exchanged into deuterated HEPES buffer (50 mM, pD 7.5) to a concentration of 8–9 mM active sites (4–5 mM enzyme homodimers). CAD substrate was lyophilized for storage and added to samples of FIH in this form. Samples for spectroscopy were prepared in an anaerobic “wet box” under N₂ atmosphere. Ferrous ammonium sulfate and αKG were added in microliter quantities from anaerobic stock solutions in degassed D₂O and deuterated HEPES buffer, respectively. For cofactor and substrate binding, aliquots were added until no further spectral change was observed. Enzyme samples were saturated with sucrose for preparation of MCD cells to final enzyme-bound Fe^{II} concentrations of 8–9 mM active sites. CD spectra were taken without and with sucrose addition to ensure that the glassing agent did not perturb the Fe^{II} site.

Spectroscopic Methods. NIR (600–2000 nm) CD and MCD data were recorded on a JASCO J-730 spectropolarimeter with a liquid N₂-cooled InSb detector and an Oxford Instruments SM4000-7T superconducting magnet. Vis–UV (300–900 nm) MCD data were recorded on a JASCO J-810 spectropolarimeter with an extended S-20 photomultiplier tube and an Oxford Instruments SM4000-7T superconducting magnet. CD spectra were corrected for buffer and cell contributions, and MCD spectra were corrected for the natural CD and zero-field baseline effects by averaging the magnitudes of the positive and negative field data. VTVH MCD data were collected with a calibrated Cernox resistor (Lakeshore Cryotronics, calibrated from 1.5–300 K) inserted into the sample cell for accurate sample temperature measurement. VTVH MCD data were normalized to

the intensity maximum over all isotherms for a given wavelength, and ground-state parameters were obtained by fitting the data as previously described.^{31,32}

Computational Methods. The active site of αKG-bound FIH was modeled using the crystal structure with PDB ID 1H2N as the starting point.¹⁶ The active site was truncated, and key carbon coordinates were frozen as described in the Supporting Information (SI). DFT and time-dependent DFT (TD-DFT) calculations were performed on all active-site structures using the Gaussian 09 software package.³⁵ Geometry optimizations and single-point calculations were conducted using the spin-unrestricted BP86 functional with 10% Hartree–Fock mixing, and TD-DFT calculations were performed using the spin-unrestricted B3LYP functional. All calculations were performed under tight convergence criteria. The triple-ξ basis set 6-311G* was used to describe the Fe atom, the N and O atoms of the facial triad directly coordinated to Fe, the O atom of coordinated water, and the OC–CO₂ moiety of coordinated αKG, while all other atoms were modeled using the double-ξ basis set 6-31G*. Solvation effects were included in all calculations through the use of the polarized continuum model (PCM)³⁶ with a dielectric constant, ε = 4.0. Atomic Cartesian coordinates for all optimized structures are provided in the SI.

3. RESULTS

In the results presented below we use CD and MCD spectra taken in the near-infrared (NIR) region to detect Fe^{II} ligand field (LF) transitions that are weak and otherwise obscured by water and protein vibrational transitions in absorption spectroscopy. An analysis of the NIR MCD spectra of a series of 6C, 5C, and 4C model complexes developed in reference 32 has allowed for the determination of the coordination geometry around Fe^{II} based on the energies and splitting patterns of the LF transitions. Fe^{II} in a biologically relevant ligand coordination environment of octahedral symmetry possesses a ⁵T_{2g} ground state and ⁵E_g excited state that are split in energy by 10 Dq ≈ 10000 cm⁻¹. Six-coordinate sites in lower than octahedral symmetry (i.e., the facial triad and three water ligands) generally show two LF transitions centered around 10000 cm⁻¹ (i.e., 10 Dq) and split by Δ⁵E_g ≈ 2000 cm⁻¹. Removal of one ligand to form a 5C square pyramidal site leads to a transition at ~5000 cm⁻¹ and one above 10000 cm⁻¹. Alternatively, a 5C trigonal bipyramidal site shows one transition at less than 5000 cm⁻¹ (frequently undetectable) and another at less than 10000 cm⁻¹. A 4C tetrahedral site shows only LF transitions centered around 6000–7000 cm⁻¹ due to the significantly smaller values of 10 Dq for tetrahedral vs octahedral complexes (10 Dq (T_d) = -⁴/₉(10 Dq) (O_h)). No single Fe^{II} site exhibits more than two CD/MCD bands in the NIR region. NIR CD and MCD spectra are therefore good indicators of coordination geometry and whether or not a mixture of Fe^{II} species is present. Further, NIR VTVH MCD spectroscopy (i.e., the MCD amplitude at a given wavelength as a function of field for a fixed series of increasing temperatures plotted against βH/2kT) provides information about the ground-state splitting of the t_{2g} orbitals for a given site. A non-Kramers doublet model has been developed for the fitting of VTVH MCD data which provides ground-state spin Hamiltonian parameters δ and g_{||} which in turn are used to determine the tetragonal splitting, Δ, of the d_{xy} orbital from the {d_{xz}, d_{yz}} pair, as well as the rhombic splitting, V, of the d_{xz} and d_{yz} orbitals.³¹ This splitting of the dπ orbitals can therefore be fully characterized and, in combination with the CD/MCD transition energies, gives a complete picture of the active-site geometric and electronic structure.

NIR CD and MCD. Spectra for (Fe^{II})FIH, (Fe^{II}/αKG)FIH, and (Fe^{II}/αKG/CAD)FIH are given in Figure 2.

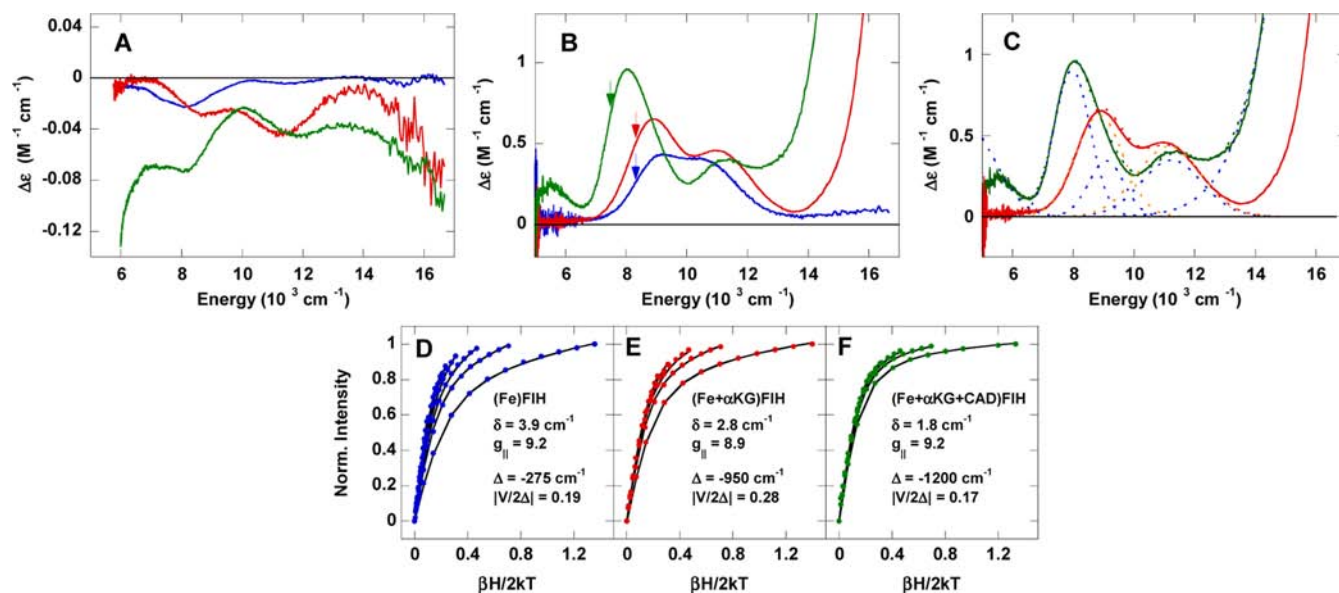


Figure 2. NIR CD, MCD, and VTVH MCD spectra of FIH. (A) The 283 K CD spectra of FIH/Fe^{II} (blue), FIH/Fe^{II}/αKG (red), and FIH/Fe^{II}/αKG/CAD (green). (B) Low-temperature (1.8 K for FIH/Fe^{II} and FIH/Fe^{II}/αKG, 3 K for FIH/Fe^{II}/αKG/CAD), 7 T MCD spectra of FIH/Fe^{II} (blue), FIH/Fe^{II}/αKG (red), and FIH/Fe^{II}/αKG/CAD (green). Arrows indicate energies for which VTVH data were collected for each sample. (C) MCD spectra of FIH/Fe^{II}/αKG (red) and FIH/Fe^{II}/αKG/CAD (green) with best fits (red dashed for FIH/Fe^{II}/αKG and green dashed for FIH/Fe^{II}/αKG/CAD) and their component peaks (orange dashed for FIH/Fe^{II}/αKG and blue dashed for FIH/Fe^{II}/αKG/CAD). VTVH data (symbols) and best fits (lines) for FIH/Fe^{II} (D), FIH/Fe^{II}/αKG (E), and FIH/Fe^{II}/αKG/CAD (F).

Table 1. ⁵E_g Energy Splittings, VTVH Parameters, and Ground-State Parameters for FIH and CS2 Species

	Fe ^{II} FIH	Fe ^{II} CS2 ^a	Fe ^{II} /αKG FIH	Fe ^{II} /αKG CS2 ^a	Fe ^{II} /αKG/CAD FIH ^b	Fe ^{II} /αKG/DGPC CS2 ^{b,d}
Δ ⁵ E _g (cm ⁻¹)	1800	1690	2300	1630	>3000 ^c	3600
δ (cm ⁻¹)	3.9	4.5	2.8	2.7	1.8	2.1
g	9.2	9.2	8.9	8.7	9.2	8.8
Δ (cm ⁻¹)	-275	-400	-950	-1000	-1200	-1300
V/2Δ (cm ⁻¹)	0.19	0.24	0.28	0.33	0.17	0.27
V (cm ⁻¹)	100	190	530	670	410	800

^aData taken from ref 26. ^bData for the 5C component. ^cCannot be exactly determined as λ_{max} of low-energy peak is not observed. ^dData taken from ref 28.

The 283 K CD spectrum of (Fe^{II})FIH (Figure 2A, blue) contains two transitions at ~8000 and 11400 cm⁻¹ (negative). Upon cooling to 1.8 K the transitions sharpen and shift to approximately 9100 and 10900 cm⁻¹ as shown in the 7 T MCD spectrum of resting FIH (Figure 2B, blue). The observed Δ⁵E_g of 1800 cm⁻¹ is typical of 6C resting αKG-dependent enzymes. Although the bands shift significantly in energy upon going from 283 to 5 K, similar behavior has been observed for the enzyme CS2 and has been attributed to stronger Fe–OH₂ bond interactions at lower temperature (the Δ⁵E_g for CS2 goes from ~2400 cm⁻¹ in the room temperature CD spectrum to ~1700 cm⁻¹ in the 5 K MCD spectrum).³³

Addition of 20 equiv of αKG to (Fe^{II})FIH produces the αKG-bound form. Both the 283 K CD and 1.8 K/7 T MCD spectra (respectively A (red) and B (red) of Figure 2) show two transitions in the ligand field region centered around 10000 cm⁻¹ split by ~2000 cm⁻¹, which imply that (Fe^{II}/αKG)FIH possesses a 6C site. While the 8400 and 11300 cm⁻¹ transitions in the CD spectrum at 283 K are similar to those of (Fe^{II})FIH, the Δε values of the (Fe^{II}/αKG)FIH transitions are appreciably larger in magnitude. At low temperature these transitions are shifted to 8900 and 11200 cm⁻¹ in the MCD spectrum. The larger band splitting observed in low-temperature MCD spectra for (Fe^{II}/αKG)FIH vs (Fe^{II})FIH (Δ⁵E_g ≈ 2300 cm⁻¹ for αKG-

bound vs 1800 cm⁻¹ for resting) is consistent with a weakening of the remaining Fe^{II}–OH₂ bond upon binding of αKG, which is a stronger donor than the two water ligands it displaces. Also visible in the MCD spectrum of (Fe^{II}/αKG)FIH is an intense positive tail on the high-energy side which comes from an Fe^{II} dπ to αKG π* metal-to-ligand charge transfer (MLCT) transition centered at ~20000 cm⁻¹ (*vide infra*).

Addition of 1.7 equiv of CAD substrate (97% loading, see SI) to (Fe^{II}/αKG)FIH produces the αKG/CAD-bound form. The CD spectrum taken at 283 K (Figure 2A, green) now has a new feature at low energy (<6000 cm⁻¹), which indicates that a square pyramidal 5C species is present in the sample. From the 3 K MCD spectrum (Figure 2B, green) three resolved peaks are visible: a low-energy feature corresponding to the shoulder in the CD spectrum at ~5500 cm⁻¹ and peaks at ~8000 cm⁻¹ and 11200 cm⁻¹. The spectrum cannot be fit without inclusion of a fourth peak at ~9000 cm⁻¹ as shown in Figure 2C. The energy positions of these four features (one low-energy and three higher-energy LF transitions) require that (Fe^{II}/αKG/CAD)-FIH is a 5C/6C mixture of two species. While one might initially consider from MCD peak positions that some unconverted αKG-bound enzyme remains, the peak area ratios of the ~9000 to 11200 cm⁻¹ features do not match between the two spectra; for the spectrum of αKG-bound FIH, the ratio is

approximately 1:1 (orange dashed lines, Figure 2C), whereas, for α KG/CAD-bound FIH, it is closer to 2:3 (blue dashed lines).

VTVH MCD. Data were collected for resting (Figure 2D), α KG-bound (Figure 2E), and α KG/CAD-bound FIH (Figure 2F). The saturation magnetization behavior for $(\text{Fe}^{\text{II}})\text{FIH}$ at $\sim 8200 \text{ cm}^{-1}$ (blue arrow in Figure 2B; note the energy used for VTVH is offset from the peak maximum to avoid overlap with the higher-energy peak) is well fit with ground-state spin Hamiltonian parameters $\delta = 3.9 \pm 0.2 \text{ cm}^{-1}$ and $g_{\parallel} = 9.2 \pm 0.1$ which correspond to $\Delta = -275 \pm 50 \text{ cm}^{-1}$ and $|V/2\Delta| = 0.19 \pm 0.02$. These small ${}^5T_{2g}$ ground-state splittings are very similar to those observed for the resting forms of other α -keto acid-dependent enzymes, where none of the ligands have particularly strong π interactions with the metal.^{28,33,37} Comparison of ΔE_g values, VTVH parameters and ground-state parameters for the (Fe^{II}) , $(\text{Fe}^{\text{II}}/\alpha\text{KG})$, and $(\text{Fe}^{\text{II}}/\alpha\text{KG}/\text{subst.})$ forms of FIH and CS2 (for comparison) are given in Table 1.

Data were chosen for the $(\text{Fe}^{\text{II}}/\alpha\text{KG}/\text{subst.})$ form of CS2 with deoxyguanidinoproclavaminc acid (DGPC) bound.^{26,28} The data for the 8900 cm^{-1} peak of $(\text{Fe}^{\text{II}}/\alpha\text{KG})\text{FIH}$ taken at $\sim 8200 \text{ cm}^{-1}$ (red arrow in Figure 2B) are well fit by the parameters $\delta = 2.8 \pm 0.2 \text{ cm}^{-1}$ and $g_{\parallel} = 8.9 \pm 0.1$ corresponding to a $\Delta = -950 \pm 50 \text{ cm}^{-1}$ and $|V/2\Delta| = 0.28 \pm 0.02$. The increased ${}^5T_{2g}$ ground-state splitting is caused by the αKG ligand which has a strong π -back-bonding interaction with the Fe^{II} ion as found previously for other α -keto dependent enzymes.^{28,33,37}

The data for the 8000 cm^{-1} peak of $(\text{Fe}^{\text{II}}/\alpha\text{KG}/\text{CAD})\text{FIH}$ taken at $\sim 7550 \text{ cm}^{-1}$ (green arrow in Figure 2B) is fit with $\delta = 1.8 \pm 0.2 \text{ cm}^{-1}$ and $g_{\parallel} = 9.2 \pm 0.1$ corresponding to a $\Delta = -1200 \pm 100 \text{ cm}^{-1}$ and $|V/2\Delta| = 0.17 \pm 0.02$. Note that from Figure 2 D to E to F the nesting of the VTVH MCD data decreases as Δ increases. This large magnitude of Δ relative to that of $(\text{Fe}^{\text{II}}/\alpha\text{KG})\text{FIH}$ is consistent with a 5C square pyramidal αKG -bound site indicating loss of water upon αKG and substrate binding. VTVH data taken at $\sim 9400 \text{ cm}^{-1}$ for CAD/ αKG -bound FIH could not be fit to any single set of parameters due to overlap with other more intense bands.

Vis–UV MCD. Spectra of $(\text{Fe}^{\text{II}}/\alpha\text{KG})\text{FIH}$ and $(\text{Fe}^{\text{II}}/\alpha\text{KG}/\text{CAD})\text{FIH}$ (red and green curves, respectively) are given in Figure 3, along with those of $(\text{Fe}^{\text{II}}/\alpha\text{KG})\text{TauD}$ and $(\text{Fe}^{\text{II}}/\alpha\text{KG}/\text{taurine})\text{TauD}$ (black and purple, respectively) for comparison.²⁸

The major feature in each spectrum at $\sim 20000 \text{ cm}^{-1}$ corresponds to an $\text{Fe}^{\text{II}} d\pi$ to $\alpha\text{KG} \pi^*$ MLCT transition.³³

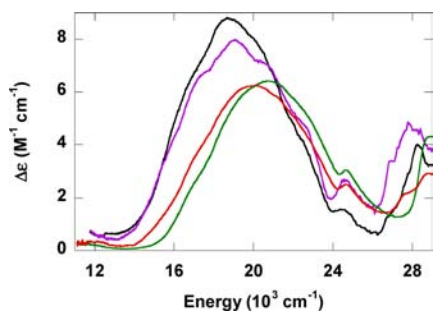


Figure 3. Vis–UV MCD spectra of αKG -bound FIH (red) and $\alpha\text{KG}/\text{CAD}$ -bound FIH (green) compared with αKG -bound TauD (black) and $\alpha\text{KG}/\text{taurine}$ -bound TauD (purple).

The $\tilde{\nu}_{\text{max}}$ of αKG -bound FIH is abnormally high at 20700 cm^{-1} . Addition of CAD substrate red-shifts $\tilde{\nu}_{\text{max}}$ to 20000 cm^{-1} . This trend is opposite of that observed for TauD, which shows a blue-shift in $\tilde{\nu}_{\text{max}}$ upon taurine binding: $(\text{Fe}^{\text{II}}/\alpha\text{KG})\text{TauD}$ and $(\text{Fe}^{\text{II}}/\alpha\text{KG}/\text{taurine})\text{TauD}$ exhibit $\tilde{\nu}_{\text{max}}$ values of 18800 and 19200 cm^{-1} , respectively. This shift of the MLCT to higher energy upon binding of substrate is commonly observed for other αKG -dependent enzymes, and has been attributed to strengthening of the $\text{Fe}^{\text{II}}-\alpha\text{KG}$ bond upon loss of coordinated water.^{20,28,38} The origin of the unusual MLCT energies in FIH and consequent implications for O_2 reactivity will be explored in the Analysis and Discussion sections, respectively.

4. ANALYSIS

Second-Sphere Interactions with the Facial Triad: Mono- vs Bidentate Coordination. From the above spectroscopic studies a H_2O is lost from the αKG -bound Fe^{II} site upon CAD substrate binding. In crystal structures of FIH (Figure 1B) the facial triad carboxylate is tilted so that its nonbonding O is pointed at the positively charged Arg238 of FIH, implying a second-sphere interaction between the two residues and a weakening of the carboxylate-ligated water H-bond which would allow the H_2O to more easily dissociate from the Fe^{II} site. In order to explore this effect on the active site, DFT computational models were constructed and their geometries optimized as shown in Figure 4 wherein Arg238 is either in its crystallographic position or moved away from the active site (by $\sim 40 \text{ \AA}$) to minimize its interaction with the carboxylate of the facial triad. Figure 4A shows that for 6C FIH the facial triad carboxylate is tilted toward positively charged Arg238 when the latter residue is in its crystallographic position. Displacement of Arg238 as in Figure 4B causes the carboxylate to tilt so as to better H-bond with the ligated water (the carboxylate O/water H distance decreases by $\sim 0.1 \text{ \AA}$). This implies that the presence of Arg238 should aid in water loss, and 5C models where the coordinated water was removed were geometry-optimized so that the effect of Arg238 could be determined (C and D of Figure 4). The following important result for the 5C forms was found: Whereas 5C FIH with Arg238 in its crystallographic position as shown in Figure 4C retains a monodentate carboxylate ligand (and is 5C as experimentally observed above), displacement of Arg238 from the active site in the absence of coordinated water leads to bidentate ligation for the facial triad carboxylate, and the $\text{Fe}^{\text{II}}-\alpha\text{KG}$ carbonyl bond weakens from $\sim 2.2 \text{ \AA}$ to 2.4 \AA (Figure 4D). Bidentate coordination in the absence of an H-bonding partner was also observed computationally for the prolylhydroxylase domain containing protein PHD2.³⁹ This finding has important implications for αKG -dependent enzymes in general and is relevant to all four classes of NH Fe^{II} enzymes. These implications are explored in the Discussion section.

Second-Sphere Interactions with the α -Keto Acid: Effects on the MLCT Transition. The MLCT transitions of $(\text{Fe}^{\text{II}}/\alpha\text{KG})\text{FIH}$ and $(\text{Fe}^{\text{II}}/\alpha\text{KG}/\text{CAD})\text{FIH}$ are significantly higher in energy than those of other αKG -dependent enzymes, and the downshift in energy upon substrate CAD binding is the opposite of what is observed for other members of the family (as seen in Figure 3). Changes in MLCT energies are due to shifts in the energies of either the donor ($\text{Fe}^{\text{II}} t_{2g}$) or acceptor ($\alpha\text{KG} \pi^*$) orbitals, both of which have an effect on the reactivity of the active site. In order to determine the cause of the unusual MLCT energies of $(\text{Fe}^{\text{II}}/\alpha\text{KG})\text{FIH}$ and energy

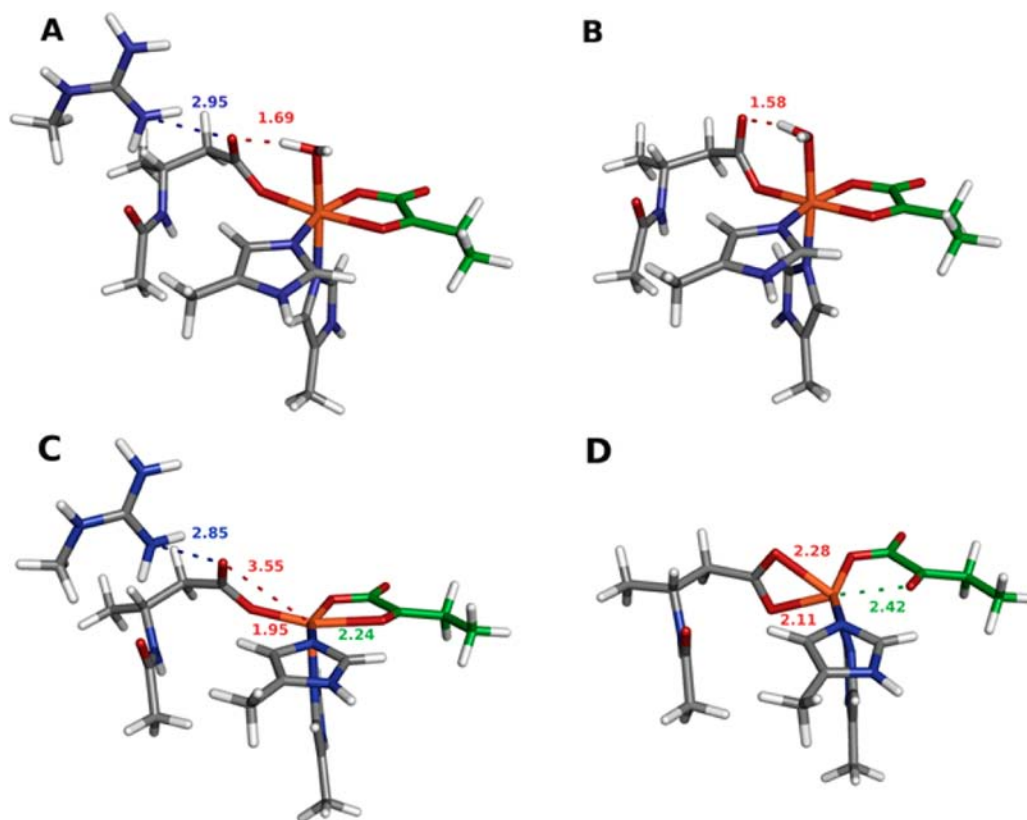


Figure 4. DFT optimized structures of FIH, showing the effects of Arg238 displacement on 6C ((A) and (B)) and 5C (C) and (D)) forms. Arg-238-facial triad carboxylate heavy atom distance in blue, facial triad carboxylate O–Fe^{II} and O–H distances in red, and α KG carbonyl O–Fe^{II} distance in green. All distances are measured in Å.

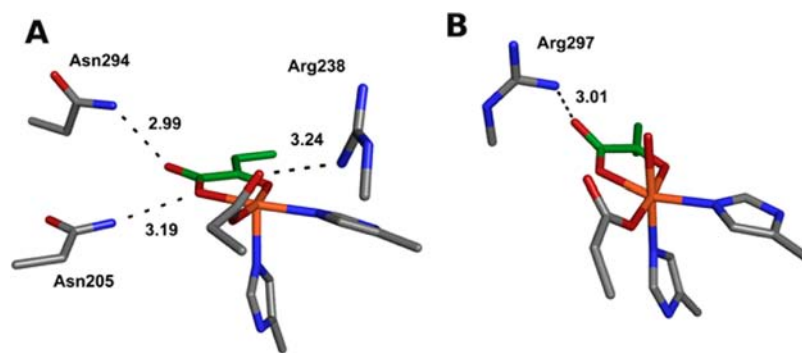


Figure 5. α KG H-bonding effects on MLCT. (A) Crystal structure of CAD-bound FIH with Arg238, showing H-bonds between the α KG carboxylate and FIH residues Asn205 and Asn294. (B) Crystal structure of clavaminase showing an H-bond between the α KG carboxylate and Arg297. All distances are in Å.

downshift of (Fe^{II}/ α KG/CAD)FIH as well as implications for reactivity, the crystal structures for FIH as well as two other α KG-dependent enzymes, CS2⁴⁰ and TauD,⁴¹ were examined to determine differences in local environments around the α KG Fe^{II} moiety. One particularly interesting structural feature of both CS2 and TauD is that the arginine, which in FIH (Arg238) is H-bonding with the facial triad carboxylate (Figure 5A), is instead located near and H-bonding with the carboxylate of the coordinated α KG, as can be seen for the CS2 structure shown in Figure 5B (Arg297).

To explore the effects of α KG carboxylate H-bonding on MLCT energy, TD-DFT calculations were performed with Arg238 in its crystallographic position (as in Figure 5A) and a model where this residue was shifted to H-bond with α KG as in

TauD and CS2 (Figure 5B). The calculated transition energies for the H₂O-ligated 6C forms for both models are given in A of Table 2.

Comparison of 6C forms with Arg238 in the FIH vs the CS2/TauD position shows that the MLCT of the former is higher in energy by ~ 2500 cm⁻¹, similar to the difference in MLCT energies between FIH and TauD (~ 1900 cm⁻¹ in Figure 3). This red-shift in the MLCT transition with H-bonds to the α KG reflects the stabilization of the α KG π^* orbital. Also as can be seen for both models in B and C of Table 2, the loss of water increases the MLCT energy by ~ 1600 cm⁻¹. This blue-shift of the MLCT has been experimentally observed for TauD^{20,28} and is due to the loss of the water ligand causing the Z_{eff} of Fe^{II} to increase, thus shifting the d orbital manifold down

Table 2. TD-DFT Energies for the Fe/ α KG π^* MLCT of Various Models to Show the Effects of α KG Carboxylate H-Bonding

	form	MLCT ^e
A ^a	Arg in FIH position, 6C	13100
	Arg in CS2/TauD position, 6C	10600
	difference (Arg in CS2/TauD pos.)	-2500
B ^b	Arg in FIH position, 6C	13100
	Arg in FIH position, 5C	14800
	difference (remove H ₂ O, FIH)	1700
C ^c	Arg in CS2/TauD position, 6C	10600
	Arg in CS2/TauD position, 5C	12100
	difference (lose H ₂ O, CS2/TauD)	1500
D ^d	Arg in FIH position, 6C	13100
	Arg in FIH position, 5C, with Asn's	13900
	difference (lose H ₂ O, add Asn's)	800

^aThe MLCT effect of shifting Arg 238 to the CS2/TauD position.

^bEffect of water loss from the FIH model. ^cEffect of water loss from the CS2/TauD model. ^dCombined effects of water loss and addition of Asn205 and Asn294 α KG carboxylate H-bonds. ^eAll energies are in cm⁻¹.

in energy, though the experimental shift is significantly smaller in magnitude (400 cm⁻¹) than that calculated (1600 cm⁻¹). However, a shift in the opposite direction is observed for FIH (Figure 3), as binding the CAD substrate with the associated loss of the water ligand causes the MLCT transition to shift down in energy.

From crystallography on FIH, there appears to be a change in H-bonding to the α KG carboxylate group, depending on whether CAD is bound or not.^{16,30,42} In crystal structures of CAD-bound FIH where either α KG (PDB ID 1H2L) or N-oxalylglycine (PDB ID 1H2K) are coordinated to Fe^{II} (N-

oxalylglycine is an inhibitor which is structurally similar to α KG and coordinates to Fe^{II} through carboxylate and α -amide carbonyl oxygens), the carboxylate of the coordinated α KG/N-oxalylglycine H-bonds with Asn205 and Asn294 of FIH as shown in Figure 5A. Alternatively, in structures of FIH where α KG (or a structural analogue) is bound (but substrate is not) these H-bonds appear to be weakened or absent (see SI). This reduced H-bonding relative to the CAD-bound forms appears to relate to the conformational flexibility of FIH residues Asn205, Asn294, and Trp296 (see SI). The flexibility of Trp296 and the asparagines appears to weaken the H-bonds to the α KG carboxylate, but upon binding substrate these residues are held in a configuration where the H-bonding is stronger. When Asn205 and Asn294 were added to the 5C FIH computational model in their 1H2L locations (Figure 5A), the MLCT transition was lowered in energy by \sim 900 cm⁻¹ (Table 2D). This MLCT energy decrease combined with the fact that the calculations significantly overestimate the increase in MLCT energy upon water loss suggests that the increase in H-bonds to the α KG carboxylate provides an explanation for the observed shifts in MLCT transition energy for FIH. That the energy of the 5C FIH MLCT is higher than that of 5C TauD by \sim 800 cm⁻¹ experimentally (compare green with purple in Figure 3) is consistent with the asparagines of FIH being neutral and stabilizing the α KG π^* orbital less than the positively charged arginine present in TauD and CS2. Consistent with the above explanation, in variants where Asn205 or Asn294 were mutated into alanine (N205A and N294A) the MLCT is shifted up in energy by \sim 500 cm⁻¹.¹⁷ The stabilization of the α KG π^* orbital through H-bonding would enhance active-site reactivity with O₂, as discussed below.

Table 3. Enzyme-Based H-Bonding Partners for the Facial Triad Carboxylate and Facial Triad Carboxylate O-Fe Bond Distances for Members of the Four Mononuclear Non-Heme Fe Enzyme Families

family	enzyme	form	PDB ID ^a	H-bonding residue(s) (distance, Å)	Fe-RCO ₂ distances (Å)
α KG-dependent	clavamate synthase	Fe/ α KG	1DS1 ⁴⁰	Y299 (2.68)	2.06, 3.39
		Fe/ α KG/PC	1DRT ⁴⁰	Y299 (2.72)	2.07, 3.44
	AlkB	Mn/ α KG	3I3Q ⁴⁷	R210 (2.86, 2.87)	2.14, 3.37
		Fe/ α KG/DNA	3I2O ⁴⁷	R210 (2.87, 2.87)	2.09, 3.24
	anthocyanidin synthase	Fe/ α KG/AN	1GP5 ⁴⁸	T239 (2.88)	2.25, 3.33
	carbapenem synthase	Fe/ α KG	1NX4 ⁴⁹	Q269 (3.10)	2.07, 3.00
		Fe/ α KG/N7P	1NX8 ⁴⁹	Q269 (3.10)	2.10, 3.30
	HPPD	Fe	1SQD ⁵⁰	Q358 (2.71)	2.17, 3.78
		Fe/869B inhib.	1TFZ ⁵⁰	Q358 (2.76)	2.02, 3.46
	HMaS	Fe/4-OH MA	2RSV ⁵¹	Q305 (2.68)	2.10, 3.59
extradiols	2,3-DHBP	Fe	1KW3 ⁵²	S247 (2.81)	2.01, 3.57
		Fe/DHBP	1KW6 ⁵²	S247 (2.72), H240 (2.66)	1.99, 3.70
	HPCD	Fe	2IG9 ⁵³	H248 (2.77)	2.05, 3.58
pterin-dependent	phenylalanine hydroxylase	Fe/HPC	1QOC ⁵⁴	H248 (2.80)	2.07, 3.58
		Fe/BH4	1J8U ⁵⁵	N/A	2.06, 3.15
		Fe/BH4/Thyl Ala	1MMK ⁵⁶	N/A	2.43, 2.44
		Fe/BH4/norleucine	1MMT ⁵⁶	N/A	2.29, 2.40
Rieske	naphthalene dioxygenase	Fe	1O7W ⁵⁷	N/A	2.27, 2.38
		Fe/naphthalene	1O7G ⁵⁷	N/A	2.26, 2.43
	biphenyl dioxygenase	Fe	3GZY ⁵⁸	N/A	1.97, 2.38
		Fe/biphenyl	3GZX ⁵⁸	N/A	2.23, 2.45
	carbazole dioxygenase	Fe	1WW9 ⁶¹	N330 (2.86)	2.10, 2.70
		Fe/carbazole	2DE7 ⁶²	N330 (2.70)	2.00, 2.70

^aReference citations given as superscripts.

5. DISCUSSION

Although crystallographic studies of (Fe^{II}/αKG)FIH and spectroscopic studies of (Co^{II}/αKG)FIH indicated that the enzyme could possess a 5C site in the presence of cofactor but absence of CAD, our MCD spectroscopic results show that in solution (Fe^{II}/αKG)FIH does not have a 5C component. This MCD spectroscopic finding for the αKG-bound site is in agreement with the general mechanistic strategy observed for mononuclear non-heme ferrous enzymes, where an open coordination position for O₂ binding is not available until both the substrate and cofactor supplying extra electrons are in their correct positions.⁴ If a significant fraction of αKG-bound Fe^{II} sites were to be 5C in the absence of substrate, uncoupled αKG turnover could take place, which would lead to autoxidation/hydroxylation and deactivation of the enzyme.

The MCD spectrum of (Fe^{II}/αKG/CAD)FIH shows that in the presence of αKG and substrate the Fe^{II} site is a mixture of 6C and 5C forms, again in accordance with our results for other α-keto-acid-dependent enzymes. This result suggests that the site is fine-tuned to release the aquo ligand from the Fe^{II} center upon substrate binding, but not to the extent that steric crowding prevents O₂ accessibility.

The facial triad carboxylate of FIH has a second-sphere interaction with its Arg238 residue (Figure 1). Removal of Arg238 from the active site of CAD-unbound FIH in computational models led the facial triad carboxylate to switch from mono- to bidentate coordination (Figure 4D), resulting in a significant weakening of the Fe^{II}–αKG carbonyl bond. The functional significance of this residue is shown in activity assays, where the R238 M mutant was inactive.¹⁷

These computational findings have strong implications for other αKG-dependent enzymes. Conversion to this bidentate form would limit O₂ reactivity as the bidentate carboxylate would block the coordination position of the Fe^{II}, and the longer, weaker Fe–αKG carbonyl bond would make formation of the Fe^{IV}-peroxo bridge⁴³ and subsequent formation of an Fe^{IV}-oxo species^{44–46} difficult and together greatly increase the reaction energy barrier. Therefore, for αKG-dependent enzymes it appears crucial to avoid bidentate coordination by the facial triad carboxylate once the coordinated H₂O is lost. To determine if other members of the αKG-dependent family have counterparts to FIH Arg238 which would prevent bidentate carboxylate coordination, crystal structures for a number of the αKG-dependent enzymes were analyzed as presented in Table 3.^{40,47–51} All of the structures show an enzyme residue positioned to H-bond with the facial triad carboxylate, which thus remains monodentate upon αKG and substrate binding and leaves an open coordination site for catalysis.

These findings prompted us to extend our study of crystal structures to other non-heme Fe^{II} enzyme families in order to determine if they had similar H-bond partners as well. The results of this analysis are included in Table 3.

Like the αKG-dependent enzymes, members of the extradiol dioxygenase family possess H-bonding partners for the facial triad carboxylate, keeping the latter monodentate.^{52–54} Both families require their electron sources to bind Fe^{II} in a bidentate fashion (in the case of the extradiol dioxygenases, as well as α-keto-acid-dependent HPPD and HMaS, the substrate also provides the electron source). This ligation requirement combined with the need for an open coordination position for O₂ to bind and be activated by Fe^{II} means that members of these families need three of the six Fe^{II} coordination sites

available for cofactor/redox-active substrate and O₂ binding as shown in Figure 6A by orange squares.

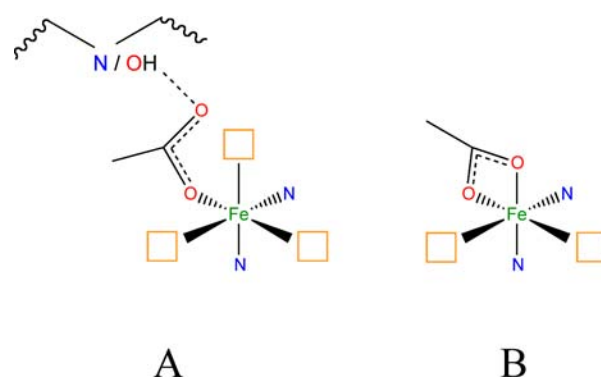


Figure 6. Fe^{II} site geometries for (A) αKG-dependent and extradiol dioxygenases and (B) pterin-dependent and Rieske dioxygenases. Orange squares denote coordination sites available for cofactor and O₂.

With the two histidines of the facial triad taking one coordination site each, the facial triad carboxylate must remain monodentate in order for O₂-activated catalysis to occur.

Alternatively, members of the pterin-dependent hydroxylases and Rieske dioxygenases generally do not have an amino acid for H-bonding with the facial triad carboxylate, and thus for these classes of non-heme Fe^{II} enzymes, this residue tends to coordinate to Fe in a bidentate fashion when substrate and cofactor are present as shown in Table 3.^{55–62} In pterin-dependent hydroxylases the tetrahydrobiopterin cofactor binds in the active-site pocket in close proximity but not directly to the Fe^{II}, while in Rieske dioxygenases the Rieske cluster and mononuclear active site are connected to each other by an H-bond network rather than being covalently linked. In these classes of non-heme iron enzymes it is beneficial to limit the number of available sites for O₂ coordination by having the facial triad carboxylate bind in a bidentate fashion as shown in Figure 6B. In the case of the pterin-dependent hydroxylases, the Fe^{IV}=O formed from a putative Fe^{II}–O₂–BH₄ bridged species must be in a position where it can attack the π cloud of the substrate. For Rieske dioxygenases, O₂ is found to coordinate to Fe in a side-on bidentate fashion in the crystal structures of an indole-bound naphthalene dioxygenase Fe–O₂ intermediate (PDB ID 1O7N)⁵⁷ as well as a carbazole-bound carbazole 1,9a-dioxygenase Fe–O₂ intermediate (PDB ID 3VMI).⁶³ This side-on O₂–Fe orientation facilitates formation of the cis-hydroxylated product as two oxygens are poised to react with substrate. Bidentate facial triad carboxylate coordination can therefore be desirable in families of enzymes where the cofactor does not coordinate to Fe^{II} to direct proper O₂ reactivity.

(Fe^{II}/αKG)FIH shows a MLCT energy of 20700 cm⁻¹, which is higher than those observed for other αKG-dependent enzymes (approximately 19000 cm⁻¹). Also, binding of CAD substrate caused the MLCT to decrease to 20000 cm⁻¹, which is the trend opposite to that observed for other members of the family (for (Fe^{II}/αKG)TauD the MLCT energy is 18800 cm⁻¹ which increases to 19200 cm⁻¹ upon binding taurine). An increase in MLCT energy upon substrate binding is calculated and expected, as there is concomitant water loss which leads to an increase in Fe^{II} Z_{eff}, thus lowering the energy of the d orbital donor manifold. However, for FIH, H-bonds are formed between enzyme residues and the carboxylate of the

coordinated α KG upon substrate binding which significantly lowers the MLCT transition energy. This lowering of the MLCT transition energy by H-bonding to the α KG carboxylate reflects the stabilization of the α KG π^* acceptor orbital in the MLCT process. This stabilization has consequences for catalysis, as the π^* orbital is involved in forming the Fe^{IV}-peroxo bridge⁴³ which precedes the decarboxylation and formation of the reactive Fe^{IV}-oxo species.^{44–46} A lower-energy π^* orbital would allow more favorable nucleophilic attack by an Fe^{IV}-peroxo species and thus lower the barrier for bridge formation. This second-sphere contribution to α KG activation is consistent with the fact that α KG-dependent enzymes generally have a residue or residues capable of forming H-bonds to the coordinated carboxylate of α KG.⁶⁴

6. CONCLUSION

In summary, this study has shown that FIH follows the same 6C \rightarrow 5C conversion as observed in the general mechanistic strategy of other non-heme Fe^{II} enzymes. Importantly, in classes of enzymes where substrate or cofactor binds to Fe^{II} (α KG-dependent and extradiol dioxygenase enzymes), second-sphere H-bonding by the protein is important in maintaining monodentate coordination of the facial triad carboxylate for O₂ coordination to Fe^{II}, while for the other classes of non-heme Fe^{II} enzymes (Rieske and pterin-dependent dioxygenases) bidentate carboxylate coordination is likely important in directing O₂ reactivity. Finally, it has been shown that the enzyme second-sphere interactions contribute to coordinated α KG activity whereby H-bonding to its carboxylate stabilizes its π^* LUMO for attack by the Fe^{IV}-peroxo in generating the Fe^{IV}=O intermediate.

■ ASSOCIATED CONTENT

■ Supporting Information

DFT geometry optimization procedure, additional CD spectra of CAD binding, table of DFT thermodynamics, coordinates for all optimized structures, additional pictures of FIH crystal structures, and full reference 35. This material is available free of charge via the Internet at <http://pubs.acs.org>.

■ AUTHOR INFORMATION

Corresponding Author

edward.solomon@stanford.edu

Notes

The authors declare no competing financial interest.

■ ACKNOWLEDGMENTS

This research was supported by NIH Grant GM 40392 (E.I.S.) and GM 077413 (M.J.K.). K.M.L. was also supported by the Althouse Stanford Graduate Fellowship; J.A.H. was supported by the CBI Training Grant (NIH T32-GM008515).

■ REFERENCES

- (1) Solomon, E. I.; Brunold, T. C.; Davis, M. I.; Kemsley, J. N.; Lee, S.-K.; Lehnert, N.; Neese, F.; Skulan, A. J.; Yang, Y.-S.; Zhou, J. *Chem. Rev.* **2000**, *100*, 235–349.
- (2) Que, L., Jr.; Ho, R. Y. N. *Chem. Rev.* **1996**, *96*, 2607–2624.
- (3) Schenk, G.; Pau, M. Y. M.; Solomon, E. I. *J. Am. Chem. Soc.* **2004**, *126*, 505–515.
- (4) Neidig, M. L.; Solomon, E. I. *Chem. Commun.* **2005**, 5843–5863.
- (5) Hegg, E. L.; Que, L., Jr. *Eur. J. Biochem.* **1997**, *250*, 625–629.
- (6) Que, L., Jr. *Nat. Struct. Biol.* **2000**, *7*, 182–184.

- (7) Koehntop, K. D.; Emerson, J. P.; Que, L., Jr. *J. Biol. Inorg. Chem.* **2005**, *10*, 87–93.
- (8) Hampton-Smith, R. J.; Peet, D. J. *Ann. N.Y. Acad. Sci.* **2009**, *1177*, 19–29.
- (9) Schofield, C. J.; Ratcliffe, P. J. *Nat. Rev. Mol. Cell Biol.* **2004**, *5*, 343–354.
- (10) Semenza, G. L. *Annu. Rev. Cell. Dev. Biol.* **1999**, *15*, 551–578.
- (11) Semenza, G. L. *Physiology* **2004**, *19*, 176–182.
- (12) Metzen, E.; Ratcliffe, P. J. *Biol. Chem.* **2004**, *385*, 223–230.
- (13) McNeill, L. A.; Hewitson, K. S.; Claridge, T. D.; Seibel, J. F.; Horsfall, L. E.; Schofield, C. J. *Biochem. J.* **2002**, *367*, 571–575.
- (14) Lando, D.; Peet, D. J.; Whelan, D. A.; Gorman, J. J.; Whitelaw, M. L. *Science* **2002**, *295*, 858–861.
- (15) Hewitson, K. S.; McNeill, L. A.; Riordan, M. V.; Tian, Y.-M.; Bullock, A. N.; Welford, R. W.; Elkins, J. M.; Oldham, N. J.; Bhattacharya, S.; Gleadle, J. M.; Ratcliffe, P. J.; Pugh, C. W.; Schofield, C. J. *J. Biol. Chem.* **2002**, *277*, 26351–26355.
- (16) Elkins, J. M.; Hewitson, K. S.; McNeill, L. A.; Seibel, J. F.; Schlemminger, I.; Pugh, C. W.; Ratcliffe, P. J.; Schofield, C. J. *J. Biol. Chem.* **2003**, *278*, 1802–1806.
- (17) Saban, E.; Chen, Y.-H.; Hangasky, J. A.; Taabazuing, C. Y.; Holmes, B. E.; Knapp, M. J. *Biochemistry* **2011**, *50*, 4733–4740.
- (18) Ehrismann, D.; Flashman, E.; Genn, D. N.; Mathioudakis, N.; Hewitson, K. S.; Ratcliffe, P. J.; Schofield, C. J. *Biochem. J.* **2007**, *401*, 227–234.
- (19) Zhou, J.; Gunsior, M.; Bachmann, B. O.; Townsend, C. A.; Solomon, E. I. *J. Am. Chem. Soc.* **1998**, *120*, 13539–13540.
- (20) Ryle, M. J.; Padmakumar, R.; Hausinger, R. P. *Biochemistry* **1999**, *38*, 15278–15286.
- (21) Matthews, M. L.; Krest, C. M.; Barr, E. W.; Vaillancourt, F. H.; Walsh, C. T.; Green, M. T.; Krebs, C.; Bollinger, J. M., Jr. *Biochemistry* **2009**, *48*, 4331–4343.
- (22) Chow, M. S.; Eser, B. E.; Wilson, S. A.; Hodgson, K. O.; Hedman, B.; Fitzpatrick, P. F.; Solomon, E. I. *J. Am. Chem. Soc.* **2009**, *131*, 7685–7698.
- (23) Ryle, M. J.; Liu, A.; Muthukumar, R. B.; Ho, R. Y. N.; Koehntop, K. D.; McCracken, J.; Que, L., Jr.; Hausinger, R. P. *Biochemistry* **2003**, *42*, 1854–1862.
- (24) Henshaw, T. F.; Feig, M.; Hausinger, R. P. *J. Inorg. Biochem.* **2004**, *98*, 856–861.
- (25) Chen, Y.-H.; Comeaux, L. M.; Herbst, R. W.; Saban, E.; Kennedy, D. C.; Maroney, M. J.; Knapp, M. J. *J. Inorg. Biochem.* **2008**, *102*, 2120–2129.
- (26) Zhou, J.; Rocklin, A. M.; Lipscomb, J. D.; Que, L., Jr.; Solomon, E. I. *J. Am. Chem. Soc.* **2002**, *124*, 4602–4609.
- (27) Rocklin, A. M.; Kato, K.; Liu, H.; Que, L., Jr.; Lipscomb, J. D. *J. Biol. Inorg. Chem.* **2004**, *9*, 171–182.
- (28) Neidig, M. L.; Brown, C. D.; Light, K. M.; Fujimori, D. G.; Nolan, E. M.; Price, J. C.; Barr, E. W.; Bollinger, J. M., Jr.; Krebs, C.; Walsh, C. T.; Solomon, E. I. *J. Am. Chem. Soc.* **2007**, *129*, 14224–14231.
- (29) To be published.
- (30) Dann, C. E., III; Bruick, R. K.; Dieshoffer, J. *Proc. Natl. Acad. Sci. U.S.A.* **2002**, *99*, 15351–15356.
- (31) Solomon, E. I.; Pavel, E. G.; Loeb, K. E.; Campochiaro, C. *Coord. Chem. Rev.* **1995**, *144*, 369–460.
- (32) Pavel, E. G.; Kitajima, N.; Solomon, E. I. *J. Am. Chem. Soc.* **1998**, *120*, 3949–3962.
- (33) Pavel, E. G.; Zhou, J.; Busby, R. W.; Gunsior, M.; Townsend, C. A.; Solomon, E. I. *J. Am. Chem. Soc.* **1998**, *120*, 743–753.
- (34) Zhou, J.; Kelly, W. L.; Bachmann, B. O.; Gunsior, M.; Townsend, C. A.; Solomon, E. I. *J. Am. Chem. Soc.* **2001**, *123*, 7388–7398.
- (35) Frisch, M. J.; et al. *Gaussian 09*, Revision A.1; Gaussian, Inc.: Wallingford, CT, 2009.
- (36) Tomasi, J.; Mennucci, B.; Cammi, R. *Chem. Rev.* **2005**, *105*, 2999–3093.

- (37) Neidig, M. L.; Decker, A.; Choroba, O. W.; Huang, F.; Kavana, M.; Moran, G. R.; Spencer, J. B.; Solomon, E. I. *Proc. Natl. Acad. Sci. U.S.A.* **2006**, *103*, 12966–12973.
- (38) Hegg, E. L.; Whiting, A. K.; Saari, R. E.; McCracken, J.; Hausinger, R. P.; Que, L., Jr. *Biochemistry* **1999**, *38*, 16714–16726.
- (39) Wick, C. R.; Lanig, H.; Jäger, C. M.; Burzlaff, N.; Clark, T. *Eur. J. Inorg. Chem.* **2012**, *31*, 4973–4985.
- (40) Zhang, Z.; Ren, J.; Stammers, D. K.; Baldwin, J. E.; Harlos, K.; Schofield, C. J. *Nat. Struct. Biol.* **2000**, *7*, 127–133.
- (41) O'Brien, J. R.; Schuller, D. J.; Yang, V. S.; Dillard, B. D.; Lanzilotta, W. N. *Biochemistry* **2003**, *42*, 5547–5554.
- (42) Conejo-Garcia, A.; McDonough, M. A.; Loenarz, C.; McNeill, L. A.; Hewitson, K. S.; Ge, W.; Liénard, B. M.; Schofield, C. J.; Clifton, I. *J. Bioorg. Med. Chem. Lett.* **2010**, *20*, 6125–6128.
- (43) Diebold, A. R.; Brown-Marshall, C. D.; Neidig, M. L.; Brownlee, J. M.; Moran, G. R.; Solomon, E. I. *J. Am. Chem. Soc.* **2011**, *133*, 18148–18160.
- (44) Price, J. C.; Barr, E. W.; Tirupati, B.; Bollinger, J. M., Jr.; Krebs, C. *Biochemistry* **2003**, *42*, 7497–7508.
- (45) Price, J. C.; Barr, E. W.; Glass, T. E.; Krebs, C.; Bollinger, J. M., Jr. *J. Am. Chem. Soc.* **2003**, *125*, 13008–13009.
- (46) Hoffart, L. M.; Barr, E. W.; Guyer, R. B.; Bollinger, J. M., Jr.; Krebs, C. *Proc. Natl. Acad. Sci. U.S.A.* **2006**, *103*, 14738–14743.
- (47) Yu, B.; Hunt, J. F. *Proc. Natl. Acad. Sci. U.S.A.* **2009**, *106*, 14315–14320.
- (48) Wilmouth, R. C.; Turnbull, J. J.; Welford, R. W. D.; Clifton, I. J.; Prescott, A. G.; Schofield, C. J. *Structure* **2002**, *10*, 93–103.
- (49) Clifton, I. J.; Doan, L. X.; Sleeman, M. C.; Topf, M.; Suzuki, H.; Wilmouth, R. C.; Schofield, C. J. *J. Biol. Chem.* **2003**, *278*, 20843–20850.
- (50) Yang, C.; Pflugrath, J. W.; Camper, D. L.; Foster, M. L.; Pernich, D. J.; Walsh, T. A. *Biochemistry* **2004**, *43*, 10414–10423.
- (51) Brownlee, J.; He, P.; Moran, G. R.; Harrison, D. H. T. *Biochemistry* **2008**, *47*, 2002–2013.
- (52) Sato, N.; Uragami, Y.; Nishizaki, T.; Takahashi, Y.; Sasaki, G.; Sugimoto, K.; Nonaka, T.; Masai, E.; Fukuda, M.; Senda, T. *J. Mol. Biol.* **2002**, *321*, 621–636.
- (53) Kovaleva, E. G.; Lipscomb, J. D. *Science* **2007**, *316*, 453–457.
- (54) Vetting, M. W.; Wackett, L. P.; Que, L., Jr.; Lipscomb, J. D.; Ohlendorf, D. H. *J. Bacteriol.* **2004**, *186*, 1945–1958.
- (55) Andersen, O. A.; Flatmark, T.; Hough, E. J. *Mol. Biol.* **2001**, *314*, 279–291.
- (56) Andersen, O. A.; Stokka, A. J.; Flatmark, T.; Hough, E. J. *Mol. Biol.* **2003**, *333*, 747–757.
- (57) Karlsson, A.; Parales, J. V.; Parales, R. E.; Gibson, D. T.; Eklund, H.; Ramaswamy, S. *Science* **2003**, *299*, 1039–1042.
- (58) Colbert, C. L.; Agar, N. Y.; Kumar, P.; Chakko, M. N.; Sinha, S. C.; Powlowski, J. B.; Eltis, L. D.; Bolin, J. T. *PLoS ONE* **2013**, *8*, No. e52550, <http://www.plosone.org/article/info:doi/10.1371/journal.pone.0052550>. Accessed March 22, 2013.
- (59) In addition, the pterin-dependent enzyme tyrosine hydroxylase was shown through EXAFS to have bidentate carboxylate coordination when both tetrahydrobiopterin and substrate are bound. See ref 22).
- (60) A possible exception is the Rieske dioxygenase family member carbazole dioxygenase, which has an asparagine available for H-bonding to the facial triad carboxylate and carboxylate O–FeII bond lengths of ~2.0 and 2.7 Å. See refs 61, 62.
- (61) Nojiri, H.; Ashikawa, Y.; Noguchi, H.; Nam, J.-W.; Urata, M.; Fujimoto, Z.; Uchimura, H.; Terada, T.; Nakamura, S.; Shimizu, K.; Yoshida, T.; Habe, H.; Omori, T. *J. Mol. Biol.* **2005**, *351*, 355–370.
- (62) Ashikawa, Y.; Fujimoto, Z.; Noguchi, H.; Habe, H.; Omori, T.; Yamane, H.; Nojiri, H. *Structure* **2006**, *14*, 1779–1789.
- (63) Ashikawa, Y.; Fujimoto, Z.; Usami, Y.; Inoue, K.; Noguchi, H.; Yamane, H.; Nojiri, H. *BMC Struct. Biol.* **2012**, *12*, No. 1472-6807/12/15, <http://www.biomedcentral.com/1472-6807/12/15>. Accessed December 23, 2012.
- (64) Hangasky, J. A.; Taabazuing, C. Y.; Valliere, M. A.; Knapp, M. J. *Metallomics* **2013**, *5*, No. mt/c3mt20153h, <http://pubs.rsc.org/en/content/articlelanding/2013/mt/c3mt20153h>, accessed March 22, 2013.